Journal of Molecular Catalysis A: Chemical 333 (2010) 128–135

Contents lists available at ScienceDirect

Journal of Molecular Catalysis A: Chemical

journal homepage: www.elsevier.com/locate/molcata

Gas-phase photocatalytic degradation and detoxification of *o*-toluidine: Degradation mechanism and Salmonella mutagenicity assessment of mixed gaseous intermediates

Taicheng An[a,*], Lei Sun[a,b], Guiying Li[a,*], Shungang Wan[a,b]

[a] State Key Laboratory of Organic Geochemistry and Guangdong Key Laboratory of Environmental Resources Utilization and Protection, Guangzhou Institute of Geochemistry, Chinese Academy of Sciences, Guangzhou 510640, China
[b] Graduate School of Chinese Academy of Sciences, Beijing 100049, China

ARTICLE INFO

Article history:
Received 23 March 2010
Received in revised form 4 October 2010
Accepted 7 October 2010
Available online 15 October 2010

Keywords:
o-Toluidine
Photocatalytic oxidation
Degradation mechanism
Mutagenicity
Ames assay

ABSTRACT

The photocatalytic degradation of toluidine over titanium oxide (TiO_2) thin films under UV irradiation was investigated. The degradation efficiency of 98.7% was obtained for a toluidine concentration of about 4500 $\mu g\,L^{-1}$ and illumination of 240 min. The degradation intermediates produced during photocatalytic oxidation were identified using Fourier transform-infrared spectrometry (FTIR) and gas chromatography–mass spectrometry (GC–MS). Only a small amount of intermediates, including phenol and toluene, were found in the gas phase. Many other trace amount intermediates, such as 2-hydroxybenzaldehyde, 2-nitrobenzaldehyde, 2-hydroxybenzenemethanol, 2-hydroxybenzoic acid, phenol etc., were detected on the TiO_2 surface. An Ames assay of the *Salmonella typhimurium* strains TA98 and TA100 was employed to evaluate the mutagenicity of toluidine and its gaseous photocatalytic degradation intermediates. With or without rat liver microsomal fraction (S9 mix) activation, neither toluidine nor its gaseous intermediates presented mutagenic activity against strains TA98 (±S9) and TA100 (−S9) at all tested doses. Toluidine, however, can induce a weak positive response to the TA100 strain with an S9 mix at doses as high as 4000 $\mu g\,plate^{-1}$. An increase of revertants per plate was obtained after 30 min photocatalysis in the TA100 strain with S9 mix. As reaction time further increased, photocatalytic technology exhibited the ability to completely and efficiently detoxify toluidine. Both our chemical analysis and toxic evaluation indicate that all mutagenic intermediates in the gas can be completely eliminated within 240 min, which further suggests that photocatalytic technology is an effective approach for degrading aromatic amines.

1. Introduction

o-Toluidine, a monosubstituted aniline, has been commercially available since its first synthesis in 1844. It is often used as an intermediate in the dye industry, as well as in a number of other applications in the fields of rubber processing, pharmaceutical production, etc. [1]. *o*-Toluidine also can be released during the manufacturing and processing of coal oil gasoline, etc. According to the International Agency for Research on Cancer (IARC, 1982), the maximum permitted exposure level to *o*-toluidine in the workplace ranges from 3 to 22 $mg\,m^{-2}$ or 5 $mg\,L^{-1}$ in those countries which have set limits [2], especially since *o*-toluidine has been demonstrated to be a carcinogen in mice and rats. In fact, aromatic amines had been recognized to be carcinogenic as far back as 1895, when Ludwig Rehn described the high incidence of bladder cancer in dye industry workers as "aniline cancer" [3]. *o*-Toluidine can also be metabolized in vivo into a number of compounds, some of which are active genotoxins [2]. Due to the various environmental concerns it raised and its adverse effects on human health, *o*-toluidine has received increasing attention in recent decades [4].

Research on organic genotoxicity has become increasingly understood with the application of bacteria [5] and mammalian cells [6] in animals, as well as through epidemiological investigations among large groups of people [7,8]. Among many assay methods, the Salmonella mutagenesis assay (Ames assay) has been conveniently and reliably used [9]. Most of the research available has focused on the genotoxicity of *o*-toluidine and its co-mutagenic action with norharman [10,11], rather than the degradation intermediates produced.

Photocatalytic technology is a highly effective method for the complete degradation of a wide spectrum of organic pollutants into less toxic or harmless compounds without selection [12–16]. Most of the previous works in this field were carried out in aqueous systems [17–19], but only limited investigations focused on

* Corresponding authors. Tel.: +86 20 85291501; fax: +86 20 85290706.
E-mail addresses: antc99@gig.ac.cn (T. An), ligy1999@gig.ac.cn (G. Li).

1381-1169/$ – see front matter © 2010 Elsevier B.V. All rights reserved.
doi:10.1016/j.molcata.2010.10.009

the evaluation the detoxification of gaseous organic pollutants. Mo et al. [20] theoretically evaluated the toxicity of the photocatalytic by-products of gas-phase toluene at indoor levels and concluded that the by-products had no negative effects to human health via the health-related index (HRI). However, HRI values do not represent a standard method. Rather, they are the user-defined sum of all HRI_i parameters (i.e., the ratio of the concentration versus its recommended exposure limit of compounds *i*). To date, few studies have been reported that experimentally assess the mutagenic change trends of volatile organic compounds (VOCs) and their gaseous mixed degradation intermediates during the photocatalytic degradation.

In this work, a typical aromatic amine, *o*-toluidine, is used as a model VOC to determine photocatalytic detoxification feasibility by chemically identifying its degradation intermediates. We aim to experimentally examine the potential mutagenicity of *o*-toluidine before and during photocatalytic degradation and evaluate the safety discharge of photocatalytic technology as compared to conventional methods for the treatment of aromatic amines. A tentative degradation pathway is also proposed to explain why photocatalytic technology is an effective method for detoxifying gaseous *o*-toluidine.

2. Materials and methods

2.1. Reagents

Dimethyl sulfoxide (DMSO) (purity: >99.9%), glucose-6-phosphate (purity: >98%) and dexon (purity: 99%) were purchased from Sigma Chemical Corp. (Saint Louis, MO, USA). 2-Aminofluorene (purity: >97.0%) was purchased from Fluka Chemical Corp. (Ronkonkoma, NY, USA). Nicotinamide adenine dinucleotide phosphate (NADP), D-biotin, L-histidine, agar, nutrient broth, and other chemicals of analytical grade were purchased from Huankai (Guangzhou, China). Rat liver enzymes (S9) and *S. typhimurium* strains, TA98 and TA100, were obtained from the Guangzhou Sanitation Prevention Station, China. *o*-Toluidine (purity: 99.5%) was purchased from Acros Organics (Geel, NV, Belgium). The methanol used in the procedures was of chromatography grade (Germany). N,O-bis (trimethylsilyl)-trifluoroacetamide (BSTFA) (purity: 98%) was obtained from Acros Organics (NJ, USA). All other reagents were used as received without further purification.

2.2. Photocatalytic characterization

Nanocrystalline titanium dioxide(TiO_2) thin films were prepared via our reported method [21] with the experimental flow chart shown in Fig. 1. All photocatalytic experiments were performed in a sealed Pyrex gas–solid reactor with a total volume of 5 L [22]. Briefly, a 125-W high-pressure mercury lamp that emits maximum radiation of 365 nm (GGZ125, Shanghai Yaming Lighting Co., Ltd.) was used as the light source. Film photocatalysts were installed facing the light source, which was sleeved in the center of a double-walled quartz cylinder. The reaction temperature was maintained at room temperature by a continuous circulation of cooling water in the quartz glass jacket around the light source (light intensity: 5.3 mW cm^{-2}). A mini-type fan stirrer at the bottom was used as the air blender for the reaction gas during the operation. For a typical experiment procedure, four identically prepared TiO_2/ITO films were installed into the reactor, which was then filled with dry air. Liquid *o*-toluidine and a small fraction of distilled water were injected into the vaporizing tube from the injection port. The vaporizing tube was heated and *o*-toluidine was allowed to vaporize, mix, and reach gas–solid adsorption equilibrium. The photocatalytic degradation of *o*-toluidine was carried out via a circulation reaction process with a gas circulation pump joining with short circulation Teflon tubing. The mixed reaction gas was circulated from bottom to top. The *o*-toluidine equilibrium concentration was about 4500 μg L^{-1} and the relative humidity was ca. 45%. Once the concentration of *o*-toluidine has stabilized, the *o*-toluidine gas was then irradiated with UV light, signaling the start of photocatalysis. Subsequently, at photocatalytic intervals of 30, 60, 120, 180, and 240 min, a portion of the gaseous samples was collected and sealed in a 1-L volumetric Teflon bag for mechanism studies. Other portions of the gaseous samples were trapped with DMSO solution for mutagenicity assessment.

2.3. Analysis

A gas chromatography (GC) (HP 5890, Series II, equipped with a split/splitless injector and a flame ionization detector) was used to analyze the concentration of gaseous *o*-toluidine before and after photocatalytic degradation. The injector temperature and the detector temperature were set at 250 and 280 °C, respectively. Gaseous samples amounting to 500 μL were taken using a 500 μL gas-tight locking syringe (Agilent, Australia) at given intervals and injected into the GC for *o*-toluidine determination in splitless mode. The typically programmed temperature of the column was maintained at 40 °C for 2 min, then increased to 100 °C at a rate of 6 °C min^{-1}, and finally increased to 280 °C at a rate of 10 °C min^{-1}. The concentrations of the target compounds were quantified by external standard calibration. The degraded gaseous intermediates were analyzed by a GC (Agilent 7890A)–mass spectrometer detector (Agilent 5975C with Triple-Axis Detector) (GC–MSD) with a DB-5 capillary column (30 m × 0.32 mm × 0.25 μm, Agilent Technology). The carrier gas was ultra-high purity helium fed at a constant flow rate of 1.3 mL min^{-1}. The analysis method and programmed procedure were the same as for GC quantification. The MSD was operated in full scan mode with *m*/*z* 40–300 amu. The gaseous target species were identified via their mass spectrum using the Wiley database (Wiley Mass Spectral Library).

To identify the intermediates adsorbed onto the surface of TiO_2 thin films, two sets of experiments were performed. First, solid intermediates deposited onto the thin films were directly analyzed by Nicolet 330 Fourier transform-infrared spectroscopy (FTIR). Next, these intermediates were extracted ultrasonically using a small amount of methanol for 30 min. The extract was filtered through a 0.45 μm filter membrane. The filtrate was collected, concentrated with a gentle stream of high-purity nitrogen, averaged into two similar 1.5 mL vials, and then completely dried with a gentle stream of high-purity nitrogen. One portion of the sample was re-dissolved in 1.0 mL ethyl acetate and then injected into the GC–MSD for the direct determination of intermediates. The remaining portion was derived at room temperature using 50 μL BSTFA as the derivatization reagent and 50 μL pyridine as the catalyst. The resulting solution was injected into the GC–MSD to identify polar intermediates. Samples amounting to 1.0 μL were injected in the splitless mode. The analysis method was the same as for the detection of gaseous target species. These intermediates were also identified via their mass spectrum according to the library spectra as described previously.

2.4. Mutagencity assessment

Ames assays were performed according to the standard plate incorporation method with the classic *S. typhimurium* strains, TA98 and TA100, which are capable of detecting base frame shift types and base pair substitution-type mutagenicity, respectively [23]. *o*-Toluidine and its photocatalytic degradation intermediates at 30, 60, 120, 180, and 240 min were trapped and dissolved completely

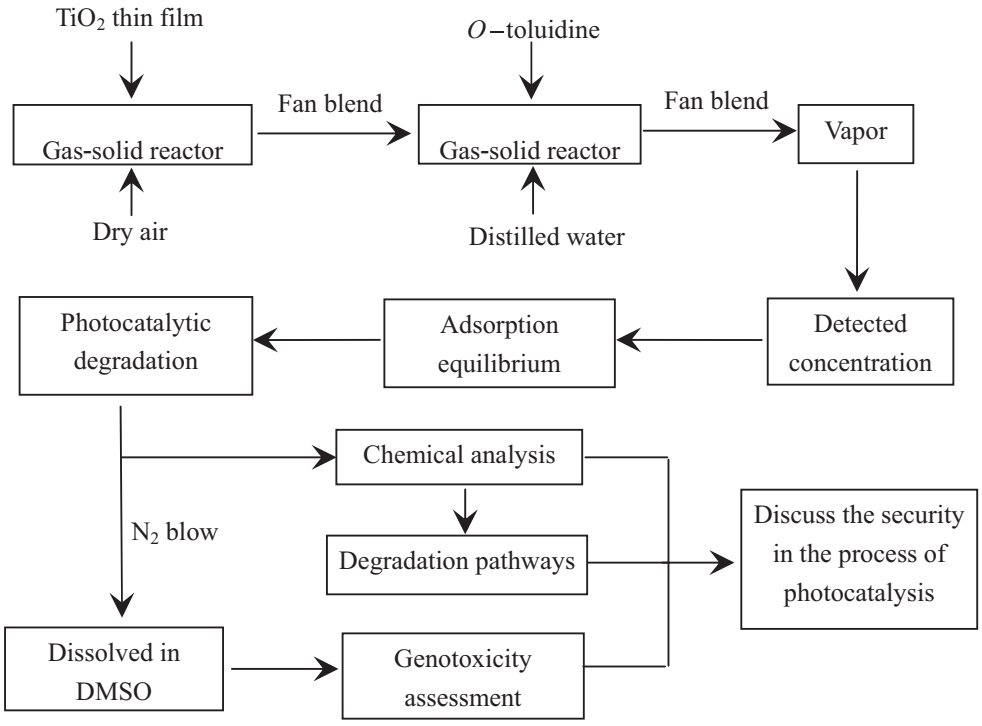

Fig. 1. Experimental flowchart.

in 5 mL of DMSO. All the experimental conditions employed were identical for both strains with and without S9 metabolic activation, except for the positive control regents used. Four different dose groups (4000, 2000, 1000, and 500 μg plate^{-1}) for each sample were assayed in triplicates. Two known mutagens, dexon and 2-aminofluorene, were used as the positive control regents without S9 and with S9, respectively. The strains were tested without the addition of any foreign compounds as negative controls. Solvent controls were also assessed for each determination. The revertant colonies on each plate were counted and scored after 48 h incubation at 37 °C, and the number of *his*$^+$ revertants in each sample was recorded as the mean value from three plates. Mutagenic index (MI) was also calculated for each dose as the ratio of the average numbers of revertants per plate in a sample and in the negative control. A sample was considered mutagenic when the MI value was equal to or greater than 2 for at least one of the tested doses and if it had a reproducible dose–response curve [24].

3. Results and discussion

3.1. Photocatalytic degradation kinetics

The photocatalytic degradation kinetics of *o*-toluidine was investigated, and the results are shown in Fig. 2. As seen in Fig. 2, gaseous *o*-toluidine can reach adsorption–desorption equilibrium after 120 min in dark conditions. This equilibrium concentration is about 4500 μg L^{-1}. *o*-Toluidine can be very slowly photolyzed under UV light irradiation in the absence of film photocatalysts with increasing reaction time. The photocatalytic efficiency of *o*-toluidine was found to be 21.2% within 240 min. In the presence of TiO_2 films, however, *o*-toluidine can be degraded with a degradation efficiency of 98.7% within the same time course. The linear plot of $\ln(C_0/C_t)$ versus time for the photocatalytic degradation is shown in the inset of Fig. 2. In a heterogeneous solid–gas reaction, the photocatalytic degradation of *o*-toluidine on the TiO_2 thin

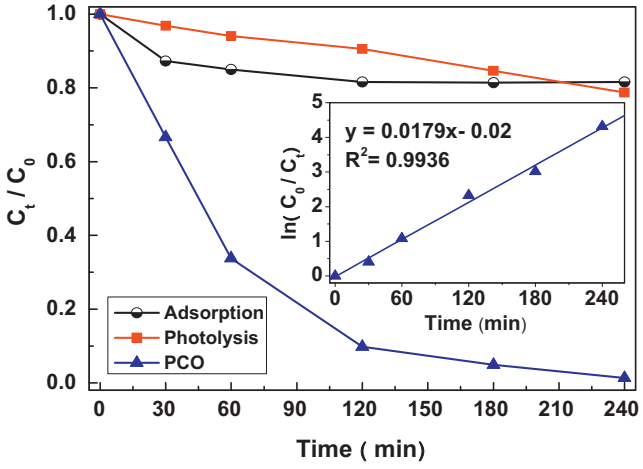

Fig. 2. Photocatalytic degradation kinetics of *o*-toluidine. Inset: linear plots of $\ln(C_0/C_t)$ versus reaction time.

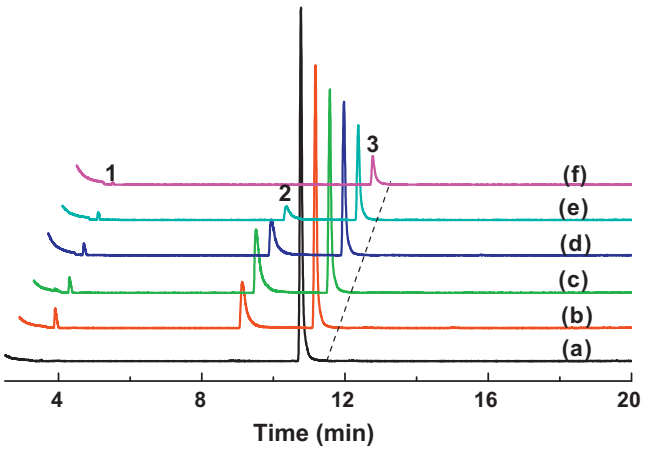

Fig. 3. TIC profile for gaseous compounds in the photocatalytic degradation of *o*-toluidine: (a) 0 min; (b) 30 min; (c) 60 min; (d) 120 min; (e) 180 min; and (f) 240 min.

film surface follows a pseudo-first-order reaction, which is consistent with the Langmuir–Hinshelwood (L–H) model. Its kinetic equation may be simplified as follows: $\ln(C_0/C_t) = kt$ [25], where k is the apparent rate constant of the photocatalytic degradation, C_0 and C_t are the initial and the final concentrations of *o*-toluidine, respectively, and t is the degradation time in minutes. Rate constant, which is the slope of the linear fit of $\ln(C_0/C_t)$ versus time, was calculated as 0.018 min^{-1}. We also calculated the half-life of our system and found it to be 38.5 min. The lower rate constant and longer half-life obtained under the same conditions indicate that *o*-toluidine was more difficult to be degraded compared to toluene, as reported in our previous work [22]. The difference in the compound structures of *o*-toluidine and toluene may have affected the extent of photocatalytic reaction observed.

3.2. Identification of the photocatalytic degradation intermediates

The resultant gaseous mixtures after gas–solid phase photocatalytic degradation were subject to GC–MSD analysis. Total ion current (TIC) profiles of gaseous compounds recorded at different reaction intervals are shown in Fig. 3. For samples without degradation (Fig. 3a), a peak (3) with retention time (t_R) of 10.9 min was observed, signifying the presence of the original *o*-toluidine molecule. For 240-min photocatalytic degradation samples, the degradation intermediates 1 (t_R = 3.7 min) and 2 (t_R = 8.8 min) were detected in the gas phase. Two most probable intermediates 1 and 2 were identified with GC–MS analysis as toluene and phenol in the air from degradation of *o*-toluidine. In the mass spectra, a couple m/z values of 92/91 corresponding to $M^+/M^+ - 1$ fragmentation of intermediates 1 was obtained with a molecule weight of toluene. Also, an m/z value of 94 corresponding to $M^+ - 1$ fragmentation of intermediates 2 also was obtained with a molecule weight of phenol. Of course, both the MS cleavage patterns of intermediates 1 and 2 also conform to that of toluene and phenol very well. During first stage of the photocatalytic degradation, the concentration of toluene in the degradation mixture decreased slightly, while the concentration of phenol increased to its maximum. When the degradation time was further increased, both toluene and phenol decreased gradually, ultimately reaching levels below detection limits after 240 min photocatalytic degradation. It must be noted that *o*-toluidine (3) remained the dominant compound, although its concentration in the reaction mixture decreased rapidly with the increase in reaction time. This indicates that *o*-toluidine can be degraded effectively, while the gaseous intermediates of toluene and phenol were produced and then degraded again during the degradation course. The plots of the concentrations of *o*-toluidine, toluene, and phenol against the reaction time are shown in Fig. 4. The equilibrium concentration of *o*-toluidine was about 4500 $\mu g\,L^{-1}$ before the photocatalytic degradation. In the gaseous mixture, the concentrations of *o*-toluidine, phenol, and toluene were 3000, 510, and 180 $\mu g\,L^{-1}$ within 30 min photocatalytic degradation, and 1520, 560, and 160 $\mu g\,L^{-1}$ after 60 min photocatalytic degradation, respectively. For 120-min photocatalytic degradation samples, the concentrations of *o*-toluidine, phenol, and toluene were 440, 250, and 86 $\mu g\,L^{-1}$, respectively. The concentration of *o*-toluidine decreased to 60 $\mu g\,L^{-1}$ and approximately 98.7% of *o*-toluidine was degraded, while both the phenol and toluene intermediates could not be detected after 240 min photocatalytic degradation. Thus, we can conclude that *o*-toluidine and both its gaseous intermediates, phenol and toluene, may be completely mineralized into CO_2 and H_2O given enough degradation time.

In order to obtain full insights into the produced intermediates involved in the reaction process, the trace solid by-products adsorbed onto the TiO_2 films were also studied by both in situ

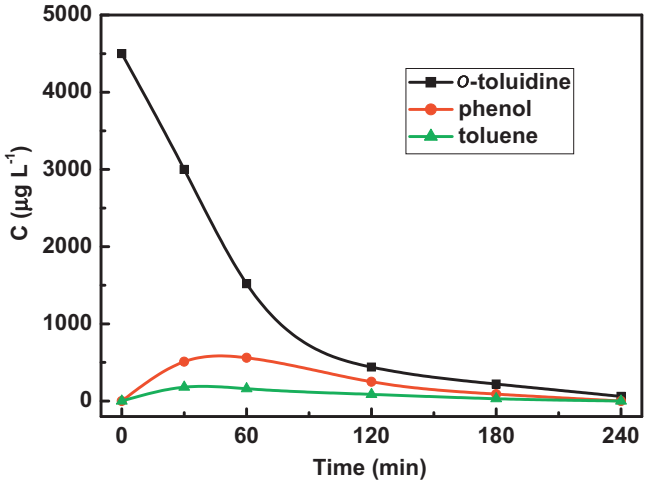

Fig. 4. The concentration conversion curve of *o*-toluidine, toluene, and phenol in the gas phase system.

FTIR spectroscopy and GC–MSD with and without BSTFA derivation. The FTIR spectra shown in Fig. 5(a)–(f) reveals the information from TiO_2 thin films before (0 min) and after photocatalytic degradation at different intervals of 30, 60, 120, 180, and 240 min. Fig. 5a shows that the spectrum of a fresh TiO_2 thin film catalyst was relatively flat. However, the trend of an initially increasing and then decreasing band was observed near 1000–1300 cm^{-1} (C–O stretching vibration) with increasing of the degradation time. The intensity of this band in the FTIR spectrum after 180-min degradation (Fig. 5e) was significantly higher than that in the other samples. Thus, we can conclude that the C–O bond may have accumulated onto the catalysts and reached maximum amounts at 180 min photocatalytic degradation. This indicated that the intermediates with C–O stretching vibration band were formed first and then subsequently mineralized with further the increases in reaction time. The intensity of the wide band at 3200–3700 cm^{-1} (OH group characteristics) also initially increased, peaked at 120 min degradation, and then decreased subsequently, indicating that the appearance and disappearance of OH group of alcohol or phenol species [26,27]. The weak band at 1680–1720 cm^{-1} was also assigned to be the C=O stretching vibration of aldehydes or carboxylic acids [28]. The weak bimodal band at 1580–1640 cm^{-1} can be recognized as the C=C stretching vibration of the aromatic ring [26]. Thus, it was deduced

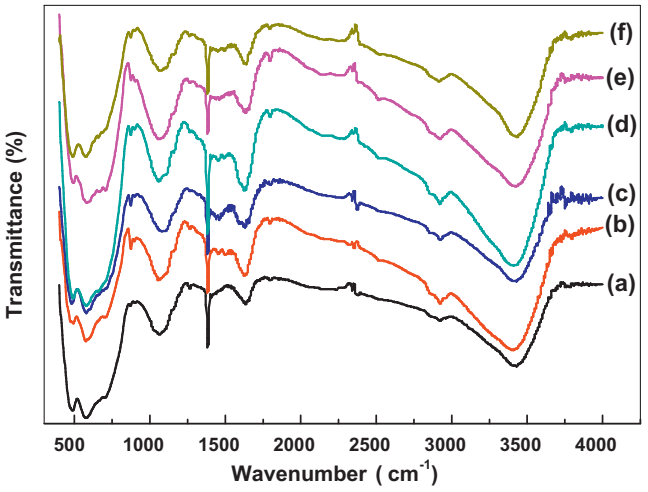

Fig. 5. FTIR spectra of TiO_2 thin films during the photocatalytic degradation: (a) 0 min; (b) 30 min; (c) 60 min; (d) 120 min; (e) 180 min; and (f) 240 min.

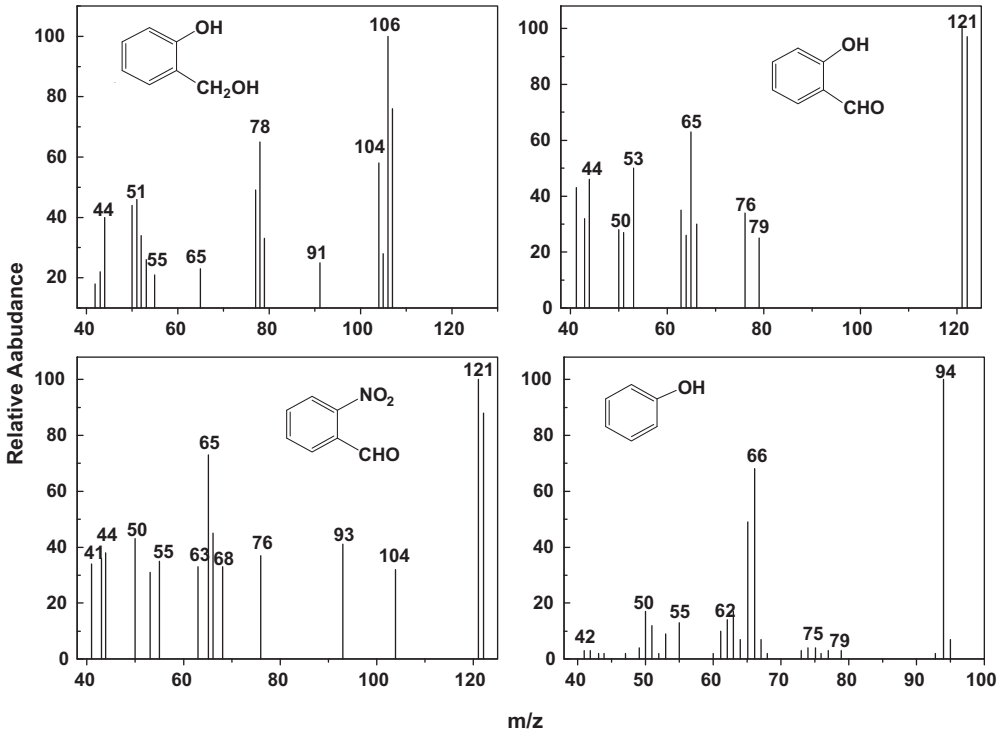

Fig. 6. Mass spectra of adsorbed intermediates on TiO_2 thin film during the photocatalytic degradation identified by GC–MS without silylation.

that the skeleton structure of the aromatic ring was still presented onto TiO_2 surfaces. It is also noted that the weak band appeared near 1350 and 1560 cm^{-1}, were assigned to be the stretching vibrations of $-NO_2$ [29,30]. These observations can be doubly confirmed by the gradual changes in color of the TiO_2 thin films: from white to pale yellow and then to yellow brown with increases in reaction time. From the analysis above, the FTIR spectra indicate that some alcohols, phenols, carboxylic acids, and nitro compounds as well as aromatic ring compounds may be produced and absorbed onto TiO_2 surfaces during the photocatalytic degradation of gaseous *o*-toluidine.

Thus, the adsorbed intermediates on the TiO_2 thin films were further confirmed with GC–MSD after extraction with methanol. The analysis results of the mass spectra of samples with and without BSTFA derivatization are shown in Figs. 6 and 7, respectively. Seen from the mass spectra of Fig. 6, besides above identified phenol, 2-hydroxybenzenemethanol, 2-nitrobenzaldehyde, and 2-hydroxybenzaldehyde were also identified in the adsorbed solid samples without BSTFA derivatization. In the mass spectra of 2-hydroxybenzaldehyde, a couple *m*/*z* values of 122/121 corresponding to $M^+/M^+ - 1$ fragmentation can be obtained. However, we cannot get the molecule ion peaks of 2-hydroxybenzenemethanol and 2-nitrobenzaldehyde of 124 and 151 from both the mass spectra, respectively. It is fortunate that we can easily find the cleave fragmentation of 106 and 78 from the mass spectra of 2-hydroxybenzenemethanol. Similarly, the cleave fragmentation of 121, 104, 76 and 65 also can be found from the mass spectra of 2-nitrobenzaldehyde. Thus, combined above FTIR spectra with mass spectra patters, all four intermediates were identified reasonably. It was also noted that all these identified intermediates were doubly confirmed with authentic standard reagents.

As the similar way, three intermediates were also found in the adsorbed solid sample with the derivative form of trimethylsiloxy ester after BSTFA derivatization (as shown in Fig. 7). In the mass spectra, a *m*/*z* value of 180 corresponding to $M^+/M^+ - 1$ fragmentation coupling with the cleave fragmentation of 165, 135 and 91 was identified as 2-methylphenyl trimethylsilyl ether. As for benzoic acid trimethylsilyl ester, a very weak molecule ion peak of 194 was also found coupling with cleavage fragmentation of 179, 147, 135 and 105. Also, as for third intermediates, salicylic acid, a *m*/*z* value of 267 was also identified as the molecule ion peak of bis(trimethylsilyl) derivative of salicylic acid after BSTFA derivatization. Thus, from above-mentioned discussion, all three intermediates were identified as 2-methylphenol, benzoic acid, and salicylic acid, respectively, in the adsorbed solid sample.

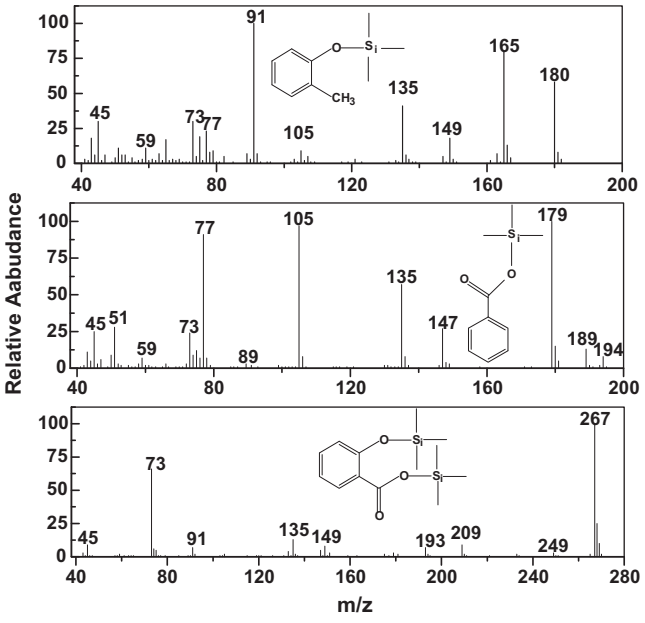

Fig. 7. Mass spectra of adsorbed intermediates on TiO_2 thin film during the photocatalytic degradation identified with BSTFA silylation.

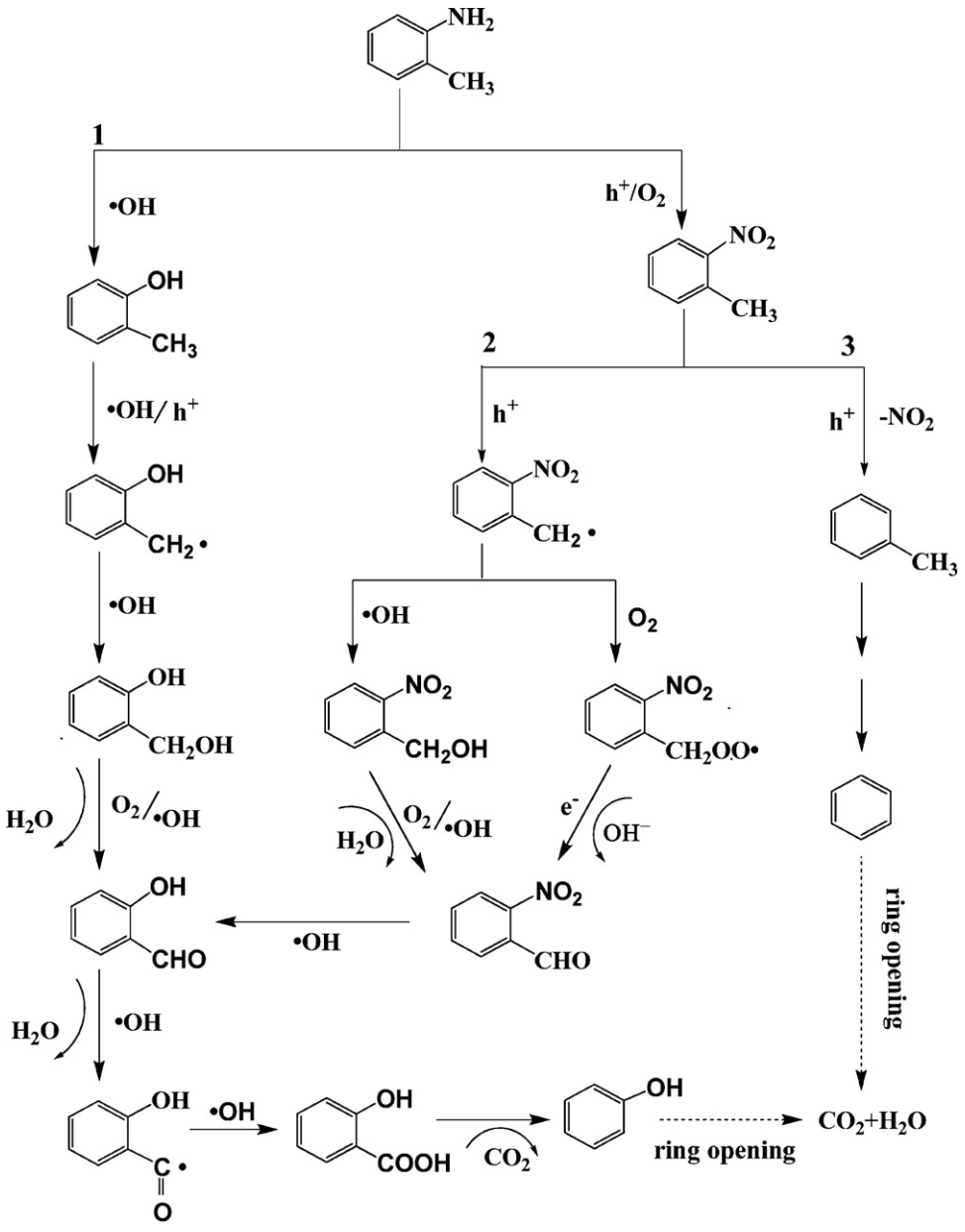

Fig. 8. Proposed photocatalytic degradation pathways for *o*-toluidine in the gas phase.

Based on the identified intermediates from both the gas and adsorbed solid phases in our experimental system, a possible photocatalytic degradation mechanism of *o*-toluidine is tentatively proposed in Fig. 8. It is suggested that three distinct pathways might occur simultaneously during the photocatalytic degradation. Following pathway 1, *o*-toluidine is oxidized to 2-methylphenol by the attack of •OH radical. Direct hydrogen abstraction by photohole from the methyl group, which leads to a benzyl radical, is followed by the formation of 2-hydroxybenzenemethanol. This compound is then further oxidized to 2-hydroxybenzaldehyde and 2-hydroxybenzoic acid. Phenols would then be produced by the photo-decarboxylation of 2-hydroxybenzoic acid [31]. In pathways 2 and 3, *o*-toluidine is first oxidized to o-nitrotoluene by photohole and oxygen. The hydrogen abstraction from the methyl group then further leads to a benzyl radical, followed by the formation of 2-nitrobenzaldehyde in pathway 2. Then, 2-nitrobenzaldehyde may be readily oxidized to 2-hydroxybenzaldehyde with the simultaneous elimination of $-NO_2$ groups because the $-NO_2$ group can be easily removed [32]. The further oxidation intermediates of 2-hydroxybenzaldehyde, 2-hydroxybenzoic acid, can be further converted into phenols followed with the decarboxylation reaction from the aromatic ring by partial mineralization. In pathway 3, o-nitrotoluene is first formed by photohole and oxygen as in the first step as the pathway 2. This intermediate can be further attacked by photoholes removing the $-NO_2$ group from aromatic ring to form the daughter intermediate, toluene. And the photocatalytic degradation mechanism of toluene in this system can be referenced in our recent publication [22].

From the viewpoint of chemical analysis, the identified degradation intermediates from both gaseous and adsorbed phase can be finally mineralized into CO_2 and H_2O, although some carcinogenic intermediates may be produced during the photocatalytic degradation of *o*-toluidine. Therefore, a mutagenicity assessment of the mixed intermediates is necessary during the course of the photocatalytic degradation.

Table 1
Results of the Ames assay during photocatalytic degradation of *o*-toluidine.

Sample	Dose (μg plate^{-1})	Number of revertants plate^{-1} in *S. typhimurium*[a]			
		TA98		TA100	
		−S9	+S9	−S9	+S9
o-Toluidine	0[b]	35 ± 5.6	39 ± 3.6	132 ± 6.0	136 ± 3.8
	500	32 ± 4.0 (0.9)	41 ± 2.3 (1.1)	134 ± 4.7 (1.0)	149 ± 8.0 (1.1)
	1000	37 ± 2.1 (1.1)	40 ± 6.7 (1.0)	133 ± 7.2 (1.0)	234 ± 4.6 (1.7)
	2000	35 ± 4.2 (1.0)	42 ± 2.9 (1.1)	140 ± 8.6 (1.1)	329 ± 17.2 (2.4)
	4000	22 ± 2.1 (0.6)	40 ± 5.9 (1.0)	132 ± 5.7 (1.0)	421 ± 7.0 (3.1)
PC 30 min	0	32 ± 3.8	41 ± 6.6	132 ± 6.6	138 ± 3.5
	500	36 ± 3.1 (1.1)	39 ± 3.1 (1.0)	131 ± 8.1 (1.0)	202 ± 8.5 (1.5)
	1000	31 ± 4.2 (1.0)	41 ± 3.5 (1.0)	134 ± 6.0 (1.0)	294 ± 14.0 (2.1)
	2000	32 ± 7.1 (1.0)	37 ± 6.2 (0.9)	140 ± 10.9 (1.1)	399 ± 11.7 (2.9)
	4000	30 ± 2.5 (0.9)	34 ± 2.9 (0.8)	138 ± 3.0 (1.0)	501 ± 18.0 (3.6)
PC 60 min	0	31 ± 1.7	34 ± 4.0	137 ± 5.0	138 ± 7.8
	500	32 ± 4.0 (1.0)	39 ± 2.1 (1.1)	139 ± 4.2 (1.0)	144 ± 6.9 (1.0)
	1000	28 ± 3.6 (0.9)	34 ± 5.5 (1.0)	142 ± 14.0 (1.0)	148 ± 10.5 (1.1)
	2000	30 ± 6.6 (1.0)	33 ± 3.8 (1.0)	143 ± 8.5 (1.0)	150 ± 9.8 (1.1)
	4000	31 ± 5.8 (1.0)	37 ± 1.2 (1.1)	139 ± 7.5 (1.0)	248 ± 12.3 (1.8)
PC 120 min	0	33 ± 3.1	40 ± 6.1	130 ± 8.0	144 ± 4.0
	500	37 ± 1.2 (1.1)	38 ± 2.9 (0.9)	137 ± 4.6 (1.1)	142 ± 8.6 (1.0)
	1000	35 ± 3.1 (1.1)	41 ± 2.6 (1.0)	141 ± 12.7 (1.1)	148 ± 5.0 (1.0)
	2000	31 ± 5.5 (0.9)	42 ± 2.6 (1.1)	132 ± 7.0 (1.0)	142 ± 8.5 (1.0)
	4000	34 ± 1.7(1.0)	42 ± 5.5 (1.1)	131 ± 4.6 (1.0)	134 ± 12.1 (0.9)
PC 180 min	0	27 ± 3.2	33 ± 3.6	136 ± 6.0	147 ± 6.4
	500	30 ± 2.6 (1.1)	35 ± 5.0 (1.1)	134 ± 4.0 (1.0)	152 ± 3.8 (1.0)
	1000	31 ± 3.0 (1.1)	31 ± 3.1 (0.9)	145 ± 13.1 (1.1)	148 ± 10.5 (1.0)
	2000	30 ± 2.1 (1.1)	38 ± 5.1 (1.2)	141 ± 8.0 (1.0)	145 ± 5.5 (1.0)
	4000	27 ± 5.0 (1.0)	32 ± 1.5 (1.0)	143 ± 12.5 (1.1)	147 ± 4.2 (1.0)
PC 240 min	0	29 ± 4.6	36 ± 6.1	133 ± 9.4	136 ± 6.1
	500	30 ± 3.2 (1.0)	41 ± 6.0 (1.1)	130 ± 10.6 (1.0)	143 ± 5.7 (1.1)
	1000	34 ± 4.7 (1.2)	30 ± 3.5 (0.8)	135 ± 5.6 (1.0)	141 ± 4.4 (1.0)
	2000	28 ± 4.5 (1.0)	34 ± 4.9 (0.9)	136 ± 8.9 (1.0)	134 ± 9.3 (1.0)
	4000	30 ± 1.5 (1.0)	35 ± 2.5 (1.0)	135 ± 5.1 (1.0)	145 ± 5.6 (1.1)
Solvent control[c]	100 (μL plate^{-1})	33 ± 6.5 (0.9)	41 ± 4.0 (1.0)	139 ± 10.6 (1.1)	134 ± 6.5 (1.0)
Positive control[d]	50	1315 ± 33.2 (37.6)		604 ± 19.9 (4.6)	
	20		2937 ± 128 (75.3)		1181 ± 67.2 (8.7)

[a] Mean ± standard deviation.
[b] Negative control.
[c] DMSO only.
[d] 50 μg plate^{-1} dexon without S9 and 20 μg plate^{-1} 2-aminofluorene with S9.

3.3. Mutagencity assay of gaseous intermediates during the degradation of o-toluidine

From our previous discussion, it is known that some carcinogenic intermediates may be produced during the photocatalytic degradation of *o*-toluidine. Considering that gaseous organic pollutants can directly endanger human health via inhalation and exposure, the Ames assay was employed to evaluate the detoxification ability of gaseous intermediates at different photocatalytic degradation intervals (Table 1). The range of spontaneous reversions (negative control) for the TA98 strain without S9 mixture metabolic activation (−S9) was at 27–35 revertants per plate, while the TA100 strain reverted spontaneously (−S9) with 130–137 revertants per plate in this study. The spontaneous reversions slightly increased with S9 mixture metabolic activation (+S9) for the TA98 strain at 33–41 revertants per plate and for the TA100 strain at 136–147 revertants per plate. For *o*-toluidine, at the highest tested dose of 4000 μg plate^{-1}, the number of revertants per plate obtained were 22 ± 2.1 (−S9) and 40 ± 5.9 (+S9) for the TA98 strain. This means that no obvious increase in the number of revertants was found for TA98 compared with the negative control. The numbers of revertants per plate obtained were 122 ± 8.5 (−S9) and 421 ± 7.0 (+S9) (MI = 3.1) for the TA100 strain. This indicates that *o*-toluidine has weak mutagenic activity against the TA100 strain in the presence of S9 metabolic activation because the MI value is greater than 2 at the 4000 μg plate^{-1} and it had a reproducible dose–response curve.

At different photocatalytic degradation intervals of 30, 60, 120, 180, and 240 min for the TA98 strain, the numbers of revertants per plate at the highest tested dose (i.e., 4000 μg plate^{-1}) were 30 ± 2.5, 31 ± 5.8, 34 ± 1.7, 27 ± 5.0, and 30 ± 1.5 without S9, and 34 ± 2.9, 37 ± 1.2, 42 ± 5.5, 32 ± 1.5, and 35 ± 2.5 with S9, respectively. All MI values were less than 2 and all the results were negative against the TA98 strain with and without S9 in all the dose groups of 4000, 2000, 1000, and 500 μg plate^{-1}, which indicate that the intermediates in the gaseous phase will not cause base frameshift-type mutagenicity to organisms. In addition, compared with the negative control in all the dose groups, no increase in the number of revertants per plate was detected for the TA100 strain without S9. However, different results were obtained for the TA100 strain with S9. For a 30 min photocatalytic degradation, the numbers of revertants per plate obtained were 501 ± 18.0 (MI = 3.6) at the 4000 μg plate^{-1}, 399 ± 11.7 (MI = 2.9) at the 2000 μg plate^{-1}, and 294 ± 14.0 (MI = 2.1) at the 1000 μg plate^{-1}. The MI values were larger than 2 for this group and a reproducible dose–response curve was obtained, indicating that the gaseous intermediates at 30 min photocatalytic degradation may cause base pair substitution-type mutagenicity to organisms in the presence of S9 metabolic acti-

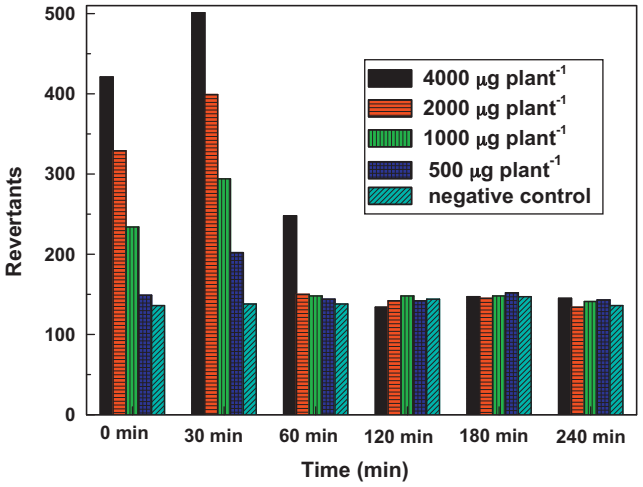

Fig. 9. Mutagenic intensity of different tested doses of raw *o*-toluidine and its intermediates to TA100 (+S9) treated at different photocatalytic degradation intervals.

vation. It was noticeable that the numbers of revertants per plate obtained for the TA100 strain with S9 decreased rapidly after 60-min photocatalytic degradation, and the MI values were all less than 2, indicating that the intermediates with mutagenicity can be subsequently photocatalytically degraded to less mutagenic new daughter intermediates with an increase in treatment time. To clearly illustrate the detoxification ability of gaseous intermediates at different photocatalytic degradation intervals, the histogram of mutagenicity intensity to TA100 (+S9) at 4000, 2000, 1000, and 500 μg plate^{-1} is shown (Fig. 9). The profiles of the mutagenic toxicity for TA100 (+S9) decreased rapidly with increases in degradation time, except for a slight increase at 30 min. The number of revertants per plate is close to the spontaneous reversions in all the dose groups after 120 min reaction. This indicates that the photocatalytic technology exhibited the ability to detoxify indirect-acting mutagenic organic pollutants efficiently, and that the gaseous outlet mixture of *o*-toluidine does not show mutagenicity to human beings and other organisms after 240 min photocatalytic degradation. The mutagenicity of the intermediates deposited onto TiO_2 thin films is not reported in this paper.

4. Conclusion

Gaseous *o*-toluidine was successfully detoxified using photocatalytic technology within a 240 min reaction, and the degradation kinetics of *o*-toluidine followed a pseudo-first-order reaction. Two intermediates of toluene and phenol were found in the gas phase. Small amounts of 2-hydroxybenzaldehyde, 2-nitrobenzaldehyde, 2-hydroxybenzenemethanol, 2-methylphenol, 2-hydroxybenzoic acid, and phenol were also identified on the surface of the thin films photocatalyst during the photocatalytic process. Furthermore, Ames assay results showed that *o*-toluidine presented weak mutagenic activity against the TA100 strain in the presence of S9 metabolic activation at tested doses. The mutagenic toxicity of its gaseous intermediates also increased slightly after a 30-min photocatalytic degradation. Finally, the samples in gas phase did not show any mutagenic activity after 240 min photocatalytic degradation. Thus, by combining our chemical analysis with the mutagenicity assessment of intermediates, we can conclude that photocatalytic technology is an effective detoxification method for *o*-toluidine in the gaseous phase. This work is of great importance in the application of photocatalytic technology for detoxifying aromatic amines in the environmental waste management field.

Acknowledgements

This is contribution No. IS-1255 from GIGCAS. This work was financially supported by the National Natural Science Foundation of China (40572173) and the Science and Technology Project of Guangdong Province, China (2007A032301002, 2009B030400001 and 2009A030902003).

References

[1] R. Stabbert, K.H. Schafer, C. Biefel, K. Rustemeier, Rapid Commun. Mass. Spectrom. 17 (2003) 2125–2132.
[2] N. Danford, Mutat. Res. 258 (1991) 207–236.
[3] R.J. Brennan, R.H. Schiestl, Mutat. Res. 430 (1999) 37–45.
[4] M.J. Plewa, T. Gichner, H. Xin, K.Y. Seo, S.R. Smith, E.D. Wagner, Environ. Toxicol. Chem. 12 (1993) 1353–1363.
[5] H.J.C. Klamer, L.A. Villerius, J. Roelsma, P.G.J. De Maagd, A. Opperhuizen, Environ. Toxicol. Chem. 16 (1997) 857–861.
[6] H.Y. Choi, Y.J. Kim, H.K. Jeon, J.C. Ryu, Mol. Cell. Toxocol. 4 (2008) 285–292.
[7] L.D. Claxton, G.M. Woodall, Mutat. Res. 636 (2007) 36–94.
[8] E. Dybing, J. O'Brien, A.G. Renwick, T. Sanner, Toxicol. Lett. 180 (2008) 110–117.
[9] L.D. Claxton, P.P. Matthews, S.H. Warren, Mutat. Res. 567 (2004) 347–399.
[10] N. Hada, Y. Totsuka, T. Enya, K. Tsurumaki, M. Nakazawa, N. Kawahara, Y. Murakami, Y. Yokoyama, T. Sugimura, K. Wakabayashi, Mutat. Res. 493 (2001) 115–126.
[11] R.L. Gupta, I.P. Kaur, A.K. Gupta, D.P. Pathak, T.R. Juneja, Toxicol. Lett. 48 (1989) 75–81.
[12] S. Artkla, W. Kim, W. Choi, J. Wittayakun, Appl. Catal. B: Environ. 91 (2009) 157–164.
[13] H. Hidaka, E. Garcia-Lopez, L. Palmisano, N. Serpone, Appl. Catal. B: Environ. 78 (2008) 139–150.
[14] A.N. Parvulescu, P.A. Jacobs, D.E. De Vos, Appl. Catal. A: Gen. 368 (2009) 9–16.
[15] Y.H. Chen, Y.Y. Liu, R.H. Lin, F.S. Yen, J. Hazard. Mater. 163 (2009) 973–981.
[16] T.C. An, G.Y. Li, X.H. Zhu, J.M. Fu, G.Y. Sheng, Z. Kun, Appl. Catal. A: Gen. 279 (2005) 247–256.
[17] M.E. Osugi, G.A. Umbuzeiro, F.J.V. De Castro, M.V.B. Zanoni, J. Hazard. Mater. 137 (2006) 871–877.
[18] G.Y. Li, T.C. An, X.P. Nie, G.Y. Sheng, X.Y. Zeng, J.M. Fu, Z. Lin, E.Y. Zeng, Environ. Toxicol. Chem. 26 (2007) 416–423.
[19] M.J. Cantavenera, I. Catanzaro, V. Loddo, L. Palmisano, G. Sciandrello, J. Photochem. Photobiol. A: Chem. 185 (2007) 277–282.
[20] J.H. Mo, Y.P. Zhang, Q.J. Xu, Y.F. Zhu, J.J. Lamson, R.Y. Zhao, Appl. Catal. B: Environ. 89 (2009) 570–576.
[21] L. Sun, T.C. An, S.G. Wan, G.Y. Li, N.Z. Bao, X.H. Hu, J.M. Fu, G.Y. Sheng, Sep. Purif. Technol. 68 (2009) 83–89.
[22] L. Sun, G.Y. Li, S.G. Wan, T.C. An, Chemosphere 78 (2010) 313–318.
[23] D.M. Maron, B.N. Ames, Mutat. Res. 113 (1983) 173–215.
[24] G. Valent, M. Sato, M. Cristina, L. Coelho, C. Coimbrao, P. Sanchez, M. Martins, R. Bonatelli Jr., Environ. Toxicol. Water Qual. 8 (1993) 371–381.
[25] M.R. Hoffmann, S.T. Martin, W.Y. Choi, D.W. Bahnemann, Chem. Rev. 95 (1995) 69–96.
[26] B. Pal, M. Sharon, J. Mol. Catal. A: Chem. 160 (2000) 453–460.
[27] C.M. Huang, G.T. Pan, P.Y. Peng, T.C.K. Yang, J. Mol. Catal. A: Chem. 327 (2010) 38–44.
[28] L.X. Cao, Z. Gao, S.L. Suib, T.N. Obee, S.O. Hay, J.D. Freihaut, J. Catal. 196 (2000) 253–261.
[29] F. Frola, F. Prinetto, G. Ghiotti, L. Castoldi, I. Nova, L. Lietti, P. Forzatti, Catal. Today 126 (2007) 81–89.
[30] S. Morandi, F. Prinetto, G. Ghiotti, M. Livi, A. Vaccari, Micropor. Mesopor. Mater. 107 (2008) 31–38.
[31] V. Augugliaro, S. Coluccia, V. Loddo, L. Marchese, G. Martra, L. Palmisano, M. Schiavello, Appl. Catal. B: Environ. 20 (1999) 15–27.
[32] W.B. Zhang, X.M. Xiao, T.C. An, Z.G. Song, J.M. Fu, G.Y. Sheng, M.C. Cui, J. Chem. Technol. Biotechnol. 78 (2003) 788–794.